Fermilab FERMILAB-Conf-00/322-E D0 August 2001

Frascati Physics Series Vol. nnn (2001), pp. 000-000
IX Int. Conf. on Calorimetry in Part. Phys. - Annecy, Oct. 9-14, 2000

DØ CALORIMETER UPGRADES FOR TEVATRON RUN II

Leslie Groer
Columbia University, New York, NY, 10027, USA

for the DØ Collaboration

ABSTRACT

The electronic readout system for the DØ liquid argon calorimeter has been upgraded to take advantage of the upcoming Tevatron Run II. New scintillation preshower detectors have been installed as well as replacements for scintillation detectors in the intercryostat regions. These upgrades and preliminary testing and calibration results are described.

1 Introduction

The DØ detector performed extremely well during the Tevatron Run I (1992-1996) and was instrumental in the discovery of the top quark [1], precision measurements of the W-boson mass [2] and many tests of the Standard Model and its extensions. The DØ detector accumulated about 125 pb^{-1} during Run I with a peak instantaneous luminosity of 1.6×10^{31} $\mathrm{cm}^{-2}\mathrm{s}^{-1}$.

The Tevatron accelerator complex at Fermilab has been upgraded with two new machines–the Main Injector and the Antiproton Recycler–both of which will contribute to substantial increases in the delivered luminosity. The Tevatron energy has also been increased from 900 GeV to 980 GeV, increasing the $p\overline{p}$ center-of-mass collisions from 1.8 TeV to 1.96 TeV.

To take advantage of these improvements and to accommodate the new beam structure, the DØ detector has undergone substantial upgrades. [3] We report here on the upgrades relevant to the calorimeter measurements.

2 DØ Detector Upgrades

In addition to the increased energy mentioned above, the Tevatron's instantaneous luminosity is expected to increase from 10^{31} cm^{-2}s^{-1} in Run I to 10^{32} cm^{-2}s^{-1} in Run II. This is made possible only by changing the beam structure and reducing the interaction time between bunch crossings. Whereas during Run I 6 p $\times$ 6 $\overline{\text{p}}$ bunches were spaced by 3.56 μs, allowing time to form trigger signals and baseline samples in between interactions, the minimal gap size in Run II will be 396 ns initially and will be reduced to 132 ns later in the run. The bunch structure also changes to that of three superbunches consisting of either 12 or 36 sub-bunches with gaps of about 2.2 μs in between the superbunches.

Fast pipelined frontend and flexible readout electronics are required to accommodate the new bunch timing which necessitated a full replacement of the DØ readout electronics and required new sophisticated trigger systems. The newly designed Level 1 (L1) trigger system operates at an input rate of 7.6 MHz with a decision time of less than 4.2 μs. The L1 trigger accept rate is fixed at 10 kHz to minimize deadtime and limited by the tracking and calorimeter readout. The L2 trigger decision time is about 100 μs with an accept rate into the L3 trigger system of about 1 kHz which should introduce no more than 5% deadtime. The L3 trigger system uses fully digitized information and has an accept rate of about 10-50 Hz to data storage.

All of the inner tracking detectors at DØ have been replaced, starting with a Silicon Microstrip Tracker (SMT) closest to the beampipe, followed by a multi-layered scintillating Central Fiber Tracker (CFT). The tracking volume sits inside a 2 Tesla magnetic field provided by a new 2.8 m superconducting solenoid. These all in turn sit inside the Central Calorimeter (CC). Attached to

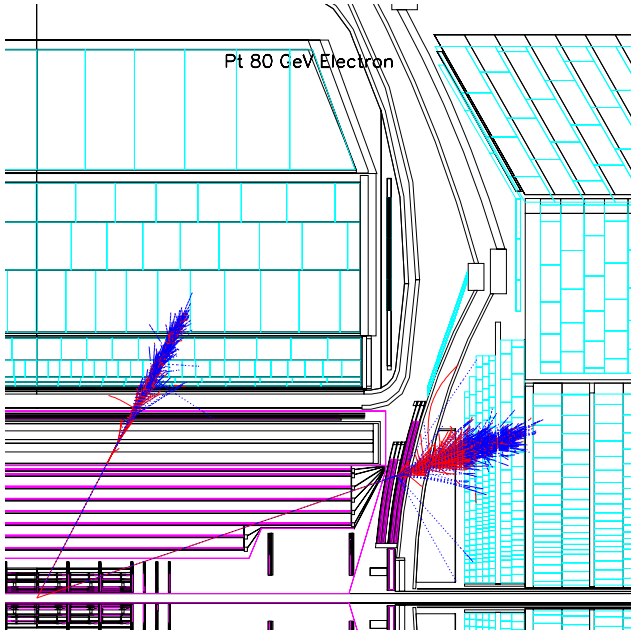

Figure 1: *Quarter cross-sectional view through the DØ Run II-detector From inside out: the Silicon Microstrip Tracker (SMT), the Central Fiber Tracker (CFT) surrounded by the solenoid, the Central and Forward Preshowers (CPS and FPS) and the Central and Endcap Calorimeters (CC and EC). The Intercryostat Detector (ICD) sits on the outside of the FPS. Simulated electrons of* $p_T = 80$ *GeV are shown traversing the central and forward regions.*

the outside of the solenoid is the Central Preshower Detector (CPS). A similar detector, the Forward Preshower Detector (FPS) and an extra scintillator based detector, the Intercryostat Detector (ICD), are placed on the inner surfaces of the two Endcap Calorimeters (EC).

Figure 1 depicts a quarter cross-sectional view of these detectors, as well as details of the inside of the calorimeter cryostats. Typical simulated high-p_T electron showers are also shown. Not shown are extensively upgraded as well as new detectors, trigger scintillators, and electronics for muon detection.

3 Preshower Detectors

The Central and Forward Preshowers serve to enhance the electron and photon identification and to sample energy after the solenoid coil, and thus provide an additional calorimetric measurement. Figure 2 shows a side-view of the two sub-detectors. They have good spatial resolution (1–2 mm) in both the $r\phi$ and rz planes to help distinguish electron, photon and pion showers.

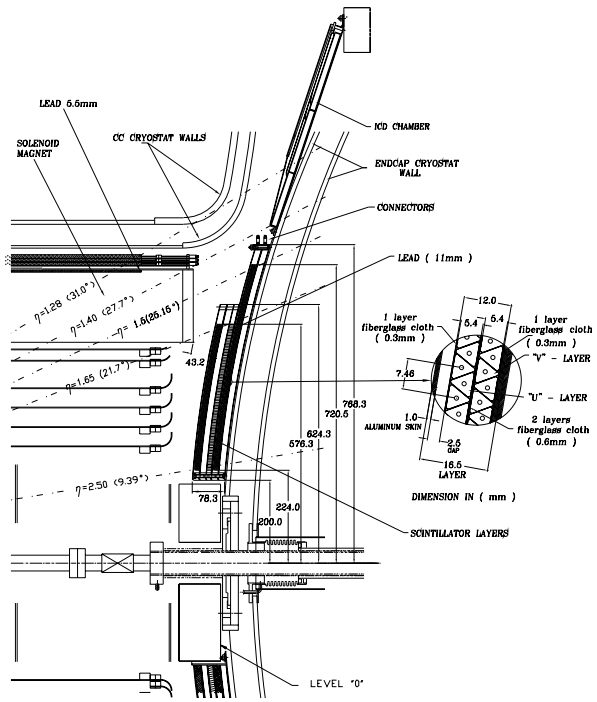

Figure 2: *rz-view of the Central and Forward Preshowers with a close-up detail of the FPS.*

The Central Preshower (CPS) [4] extends out to a pseudorapidity of $\eta = 1.3$ and is made of flat lead absorber layers attached to the solenoid and three stereo layers of scintillator strips (u, v and z). The Forward Preshower (FPS) [5] consists of two domes assembled from azimuthal wedges, mounted on the inner

cryostat of each Endcap Calorimeter and cover an $|\eta|$ range between 1.5 and 2.5. For $|\eta| > 1.65$, which corresponds to the region where particles do not encounter the solenoid, a $2X_0$ lead absorber is sandwiched in between the two domes, each dome containing two stereo layer of scintillator strips (u and v).

The readout of both preshowers is done via wavelength-shifting fibers (WLS), embedded among the scintillator strips and coupled to Visible Light Photon Counters (VLPCs) and the SVXII chip (used for the SMT and CFT readout as well) which sit in readout crates on the platform below the detector. An LED system is used for calibration.

With the introduction of the solenoid and the preshower lead converters into the cavity of the DØ tracker, the amount of material a particle encounters before hitting the first active layer of the central calorimeter has increased significantly. To illustrate, a particle originating from the primary vertex now passes through about 3.5 (5.5) X_0 of material at $\eta = 0$ (1) (as opposed to 1.5 (2.0) X_0 in Run I). The corresponding average energy loss for a 50 GeV electron before the active layer of the EM calorimeter is about 2 (7) GeV for $\eta = 0$ (1). Similarly, the FPS introduces an additional 2.2–2.5 radiation lengths in front of the first active layer of the electromagnetic EC section.

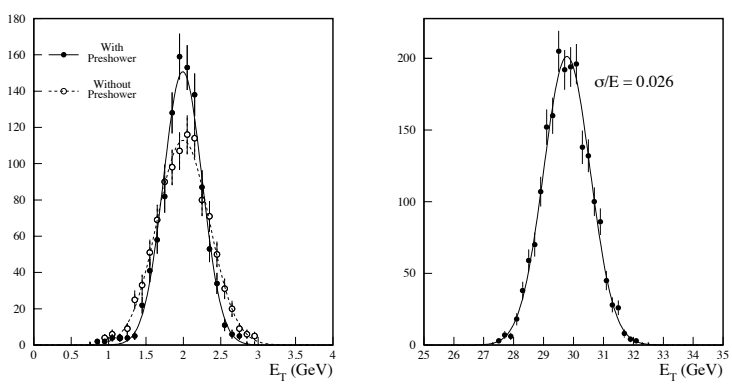

Figure 3: *Simulation of the improved electron energy resolution with the calorimeter including the Central Preshower detector for soft electrons at $E_T = 2$ GeV and the energy measurement at $E_T = 30$ GeV.*

Therefore to optimize the energy response, the contributions from the preshowers must be included. Figure 3 shows the improvement of the energy reconstruction for soft electrons with $E_T = 2$ GeV, comparing the reconstruction with and without the CPS detector. For electrons of $E_T = 30$ GeV, a resolution of $\sigma/E = 2.6\%$ is achieved. This effect is particularly marked at higher pseudorapidities ($|\eta| \approx 1$), where simulations have shown that energy resolutions can be improved by almost a factor of two ($\sigma(E)/\sqrt{E} \approx 16\%$). [6]

4 Intercryostat Detector

The rapidly changing material profile and extra uninstrumented material in the intermediate regions of the calorimeters (readout cells with no absorber material–the so called "massless gaps") leads to reduced sampling of showers and hence a degradation of energy measurements for this region. The Intercryostat Detector (ICD) [7] restores energy resolution by providing additional sampling in this region, which therefore improves the jet energy and missing energy measurements. The original Run I ICD has been entirely rebuilt with new scintillator tiles and electronics. This system will maintain the Run I performance in the presence of the magnetic field and the additional material from the solenoid.

The ICD consists of 16 supertiles per EC-region for a total of 384 scintillator tiles, covering a region of $1.1 < |\eta| < 1.4$ (see fig. 4). The tile segmentation of 0.1×0.1 in η and ϕ matches that of the calorimeter projective towers. The scintillators are read out by photomultiplier tubes (PMT) via WLS fibers. The original Run 1 PMTs are being reused (Hamamatsu R647), but due to the residual solenoidal field of a few hundred gauss in the ICD region, have to be moved to a region of reduced magnetic field. Iron boxes that house the PMTs and preamplifier circuitry sit below the calorimeter cryostats and provide some of the shielding. Clear fiber waveguides of 5–6 m are used to pipe the signal from the scintillator WLS fibers. The signal degrades by about 50% but ~ 10 photoelectrons for a single m.i.p. interaction make it to the PMT.

The readout electronics and electronic calibration scheme are the same as for the liquid argon calorimeter but with adapted electronics and pulser shapes. LED systems (adapted from the muon systems) are used to calibrate the PMTs.

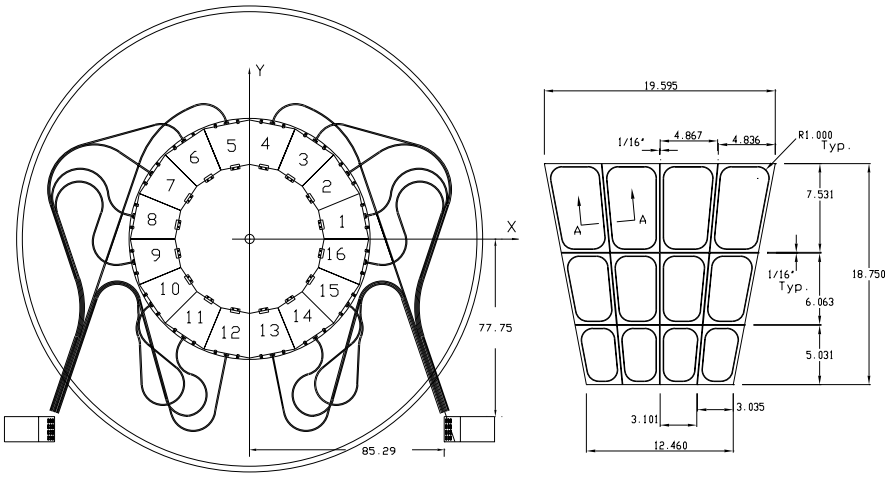

(a) (b)

Figure 4: *(a) Schematic of the ICD tile array hung on the inner surface of each Endcap Calorimeter cryostat, with the placement of the clear fiber piping to the low B-field region. (b) Schematic of the scintillator within one ICD tile module. Straight lines indicate the isolation grooves. WLS fibers are placed in the curved grooves.*

5 Liquid Argon Calorimeter

The DØ calorimeter has been described in some detail in previous calorimetry conferences [8] and is unchanged for Run II. We summarize some of the salient features in table 1. There are three liquid argon cryostats – one central (CC) and two forward/backward endcaps (EC) – which together provide complete hermetic coverage up to $|\eta| \approx 4$. Readout cells, made up of an alternating sandwich of signal boards and absorber material (uranium, copper, iron or lead) separated by a 2.3 mm liquid argon gap, are ganged into layers. The G-10 substrate for the signal boards is coated with a carbon-loaded resistive epoxy to which 2.0 kV high voltage is applied. The drift time in the liquid argon gap is about 450 ns, which sets the time scale for the signal charge collection. The readout layers are arranged into semi-projective towers of size 0.1×0.1 in $\Delta\eta \times \Delta\phi$ and are segmented longitudinally into electromagnetic (EM), fine

Table 1: *Radiation length (X_0) for readout layers in the electromagnetic (EM) and interaction lengths (λ_0) for the fine (FH) and coarse (CH) hadronic layers in the Central Calorimeter (CC) and both Endcap Calorimeters (EC).*

Layer	CC	EC
EM 1,2,3,4	X_0: 2,2,7,10 3 mm Ur	X_0: (0,3),3,8,9 (1.4 mm Fe) 4 mm Ur
FH 1,2,3,(4)	λ_0: 1.3,1.0,0.9 6 mm Ur	λ_0: 1.3,1.2,1.2,1.2 6 mm Ur
CH 1,(2,3)	λ_0: 3 46.5 mm Cu	λ_0: 3,3,3 46.5 mm Fe

hadronic (FH), and coarse hadronic (CH) sections. Projective towers consist of 8–12 layers. To capture the profile of electromagnetic showers, the third layer of the EM section, which corresponds to the shower maximum, is segmented more finely transversely into 0.05×0.05 in $\Delta\eta \times \Delta\phi$.

5.1 Upgraded Calorimeter Electronics

To accommodate the Run II bunch spacing (396 ns and later 132 ns), and to maintain the Run I noise and pile-up performance, newly designed calorimeter electronics [9] is necessary. This implied the necessity to store the analog signal for 4 μs, allowing the formation of the L1 trigger decision and to generate a separate, fast trigger signal for the calorimeter to be included in the L1 trigger level, and to adopt new strategies for the baseline subtraction.

Figure 5 sketches the calorimeter readout chain and the changes compared to the Run I setup. To minimize the sensitivity to reflections, new impedance-matched 30 Ω signal cables replace the former 110 Ω cables between the detector and the low-noise preamplifiers. The replacement cable lengths were also tuned to minimize the spread in the total cable length from the readout cells to the preamplifiers to reduce the effects of the signal timing. A fast trigger signal is then produced, whereas for the energy measurement a shaping of 400 ns is applied. Switched Capacitor Arrays (SCA) store the signal for up $\approx 4\,\mu$s until the L1 trigger decision is received. The Base-Line Subtractor (BLS) evaluates the zero-level three bunch crossings before the actual signal. New and additional controllers were needed to coordinate the 144 analog samples

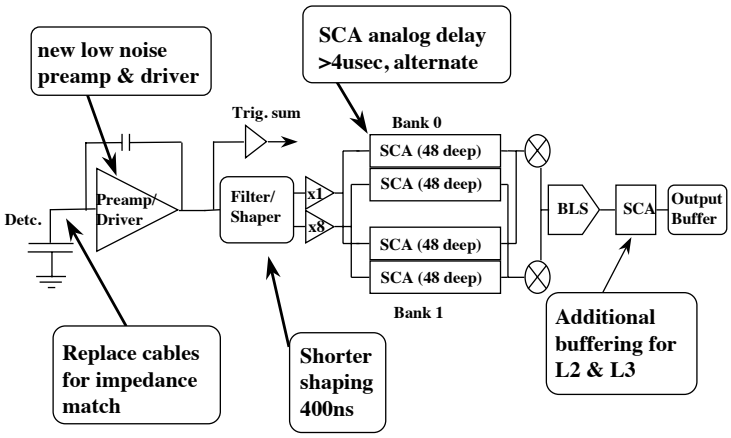

Figure 5: *Read-out chain of the calorimeter in Run II indicating the replaced or additional components compared to the Run I electronics.*

per channel. Additional buffering of the signal awaiting L2 trigger decisions is provided by supplementary SCA's. A new calibration system to accommodate the timing constraints and improve the precision has been designed. Finally, new readout electronics will be used to monitor the liquid argon purity and temperature.

The new charge-integrating preamplifier is a hybrid circuit on ceramic, similar to the Run I version. It has a high DC open-loop gain and input impedance, tuned to 30 Ω to match the input cables, and low input bias current. Two input low-noise jFETs (Toshiba 2SK369) in parallel compensate for the higher electronic thermal noise due to the shorter shaping times. To minimize reflections on the 110 Ω cable from the BLS input, the preamplifier output is terminated and back-terminated. Output driver stages have been added for terminated signal transmission and to provide current drive and differential output capability. With these additional driver stages, the preamplifier dissipates 280 mW of power compared to 80 mW in Run I.

A feedback RC circuit in the preamplifier's first stage performs a partial differentiation on the fully integrated output which compensates for the partial integration performed on the signal by the detector RC circuit, introduced by

Table 2: *Characteristics of the different Preamplifier species used for the Liquid Argon Calorimeter and the Inter Cryostat Detector.*

Preamplifier species	A	B	C	D	E	F	G	Ha-Hg	I
Avg. det. cap. (nF)	$0.26 - 0.56$	$1.1 - 1.5$	$1.8 - 2.6$	$3.4 - 4.6$	$0.36 - 0.44$	$0.72 - 1.04$	$1.3 - 1.7$	$2 - 4$	–
Layer readout	EM1,2, HAD	HAD	HAD	HAD	CC EM3	EC EM3,4	CC EM4, EC EM3,4	EC EM3,4	ICD
Feedback cap (pF)	5	5	5	5	10	10	10	10	22
RC (ns)	0	26	53	109	0	14	32	$47 - 110$	0
Total preamps	13376	2240	11008	8912	9920	7712	3232	896	384

the detector capacitance and cable impedance. The goal is to make the preamplifier output waveform as similar as possible for all channels, by customizing the preamplifier RC feedback compensation to the detector capacitances of the various cells. The characteristics of the 14 + 1 (ICD) preamplifier species that provide this compensation are shown in table 2. The ICD feedback capacitor is 22 pF to lower the gain of the output signals to preserve their dynamic range.

Forty-eight preamplifier cards are ganged together on a single motherboard, which connects into the backplane of a preamplifier box on the top of the calorimeter cryostat, which houses 96 motherboards. These are powered by low-noise commercial switching 2 kW power supplies located in steel boxes to shield the residual magnetic field of 300 gauss. The motherboard is an 8-layer printed circuit board, with ground or power planes of solid copper separating planes containing signal traces in order to minimize noise pickup and cross-talk. Calibration pulses are injected through 0.1% resistors of 10 kΩ and 20 kΩ value, depending on the preamplifier feedback capacitor.

Signals from the preamplifiers are driven over about 25 m of twisted pair cable to the Baseline Subtractor Boards (BLS) which sit in crates on the platform below the detector. The BLS board contains 4×12 signal shapers, trigger pick-off and summation circuits, 4 BLS daughterboards and output

drivers to the ADCs. Each of the BLS daughterboards holds 5 SCA chips, which are made of an array of 48 capacitors to pipeline the calorimeter signals. Two of the SCA chips, one for each of the two gain paths (×1, ×8), store the signal until the L1 trigger decision has been made, which is obtained by summation of the signals from the trigger towers. The L2 SCA buffers the data until after a L2 trigger decision and then transfers the signal to the ADC.

A simplified schematic of the SCA is shown in figure 6. The SCA is not designed for simultaneous read/write operations: two SCA banks alternate the reading and writing.

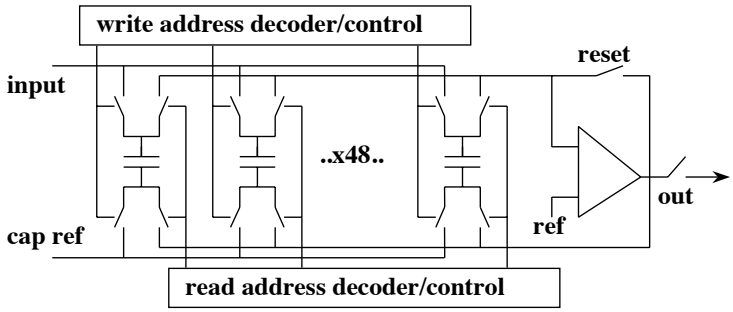

Figure 6: *Layout of the Switch Capacitor Array (SCA) which provide storage of the analog signal for up to* 4 μs.

New Timing & Control boards provide the necessary signals to handle the SCA requirements and to interface to the L1/L2 trigger systems. Each board uses three Altera FPGA chips (10K series, 208-pin packages, fastest speed version (-3), two with 20k gates and one with 30k). Three FIFO pipelines buffer up to about 40 events awaiting readout at each trigger level. Timers on these event buffers ensure that "stale" data is not sent to the data acquisition system.

The ADC successive approximation digitizers, reused from Run I, have only a 12-bit dynamic range, but a low and high gain path for each readout channel (×8/×1) maintain the 15-bit dynamic range. This matches the measured accuracy of the SCA. The readout system is approximately deadtimeless up to a L1 accept rate of 10 kHz, assuming one crossing per superbunch is read

out. The calorimeter L1 trigger is based on the energy measured in trigger towers of size 0.2×0.2 in $\Delta\eta \times \Delta\phi$, which is obtained by making appropriate sums (via resistor packs on the BLS boards) of fast pickoffs at the shaper inputs.

In order to minimize the effects of pile-up, only 2/3 of the charge in the detector is used to form the preamplifier signal. The preamplifier output is an integral of the detector signal characterized by a rise time of about 430 ns and a recovery time of 15 μs. Shaped signals are sampled every 132 ns, corresponding to 7 RF buckets from the Tevatron. The shaper circuit produces an unipolar signal with a peak at about 400 ns and a return to zero after ~ 1.2 μs. The shaped signal is sampled at 320 ns. To subtract the base-line, the signal three samples earlier is subtracted by the BLS circuitry.

5.2 Electronics Noise Performance

One of the main design goals for the Run II calorimeter electronics was to minimize the noise contributions in the new environment and to maintain the calorimeter readout performance. The shorter shaping time in Run II (from 2.2 μs to 400 ns) increases the electronics noise by a factor that scales as $1/\sqrt{t} = 2.3$ but decreases the contribution from the uranium noise and from the pile-up effects by the same factor. The pile-up contribution increases with the higher instantaneous luminosity as $\sqrt{L}$ (about a factor of 3). Finally, with the two FET input of the preamplifier giving a reduction of $\sqrt{2}$, the overall noise performance expected is about the same as that for Run I. Simulations of the benchmark W-mass measurements indicate that the calorimeter noise should not be the limiting factor.

Localized coherent noise is an issue when summing up the readout of a large number of channels, as this can affect the E_T flow. Initial measurements have been performed to check this in the readout electronics. Pedestal data were recorded in a full mock-up installation that mimics the full readout for one quadrant of a cryostat and analyzed to measure the individual channel noise (represented by the r.m.s. pedestal width in ADC counts) and the channel-to-channel correlated noise. The distribution of correlation coefficients for pairs of channels in one BLS crate is shown in figure 7. These coefficients follow a mostly Gaussian distribution with a width $\sim$0.01, as expected for a 10,000 event run. Deviations from the Gaussian are seen only at about the 0.1% level, which implies that the correlated noise between channels is minimal.

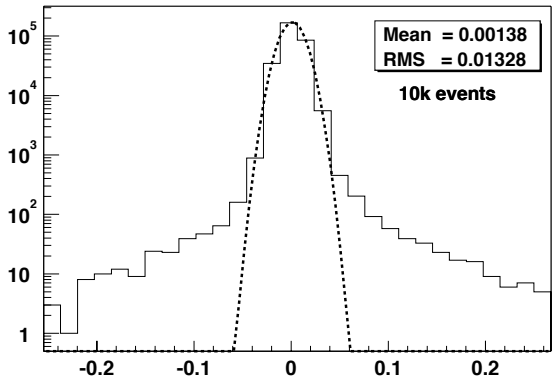

Figure 7: *Normalized pair-wise correlation coefficients based on pedestal ADC counts for all 4608 channels in one test ADC crate. The dashed line indicates a Gaussian fit to the data.*

5.3 Calorimeter Calibration System

The calorimeter calibration system consists of twelve identical units used for the liquid argon calorimeter and one slightly modified unit for the ICD. Each unit is composed of one pulser control board and its power supply, located in the BLS racks on the detector platform, and six active fanout boards, housed inside the preamplifier boxes on the cryostats. The control boards (fig. 8a) are programmed via a serial bus to a VME I/O register, which allows the amplitude and the delay of the calibration signal to be set and the selection of the channels to be pulsed. The control board delivers both a DC current, corresponding to the chosen pulse height for each selected channel, and a differential ECL command signal. The pulse heights are set via a 18-bit DAC (100 mA maximum current) and the delays are set through six programmable 8-bit delay lines with a ~ 2 ns step size. The delays allows more careful adjustment of the relative timing of the calibrated charge injection and the readout of the preamplifiers. The active fanout boards (fig. 8b) generate a pulse on the reception of a command signal. Each fanout board contains 16 switches, which convert the DC currents to precise calibration signals.

Both the pulser control board and fanout board have been tested in our

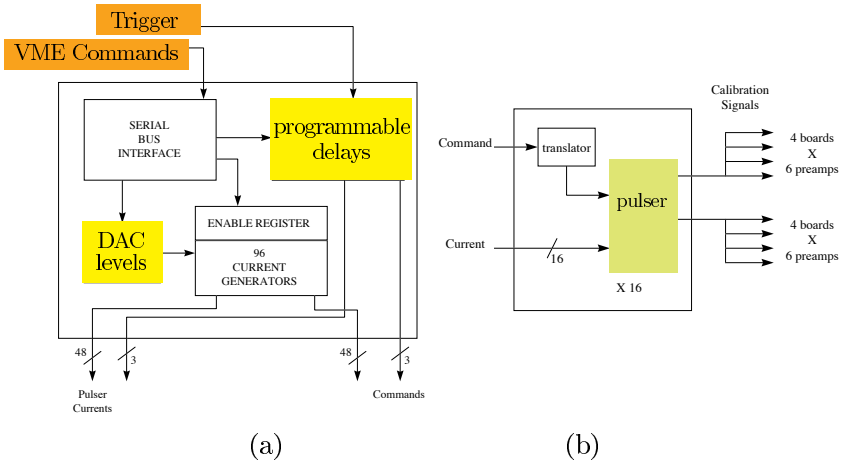

(a) (b)

Figure 8: *(a) Pulser control board set by VME, delivering DC currents and ECL commands to the fanouts. (b) Active fanout board with ECL to TTL translator and pulser-switch daughter cards, each delivering a calibration pulse to 48 preamplifier cards.*

mock-up installation and shown to provide a pulser signal with deviations from linearity on the order of $\leq 0.1\%$. All units show a uniform behavior within 0.5%. Figure 9 shows the response of the full readout chain at different pulse heights for a single channel. The linearity, defined as $(ADC_{meas.} - ADC_{fit})/ADC_{max}$ is better than 0.2% for DAC values up to 65 k. Full saturation of the ADC is observed at DAC $\sim$ 90 k, up to which essentially no noise is added from the calibration system. The cross-talk of the electronics chain was also measured while pulsing a single channel, and is below 1.5%.

Differences in the readout response to the physics signal and the calibration signal are currently being studied. These differences are due to the fact that that calibration charge is injected at the preamplifier end of the cable and not at the detector end, so some of the charge travels down the cable and reflects from the readout cell at the other end. The reflection coefficient depends on the detector capacitance at that point. Figure 10 shows the shaper output as result of a Spice simulation of the calibration signal and the physics signal for a type E preamplifier. The band indicates the changes of the output signal

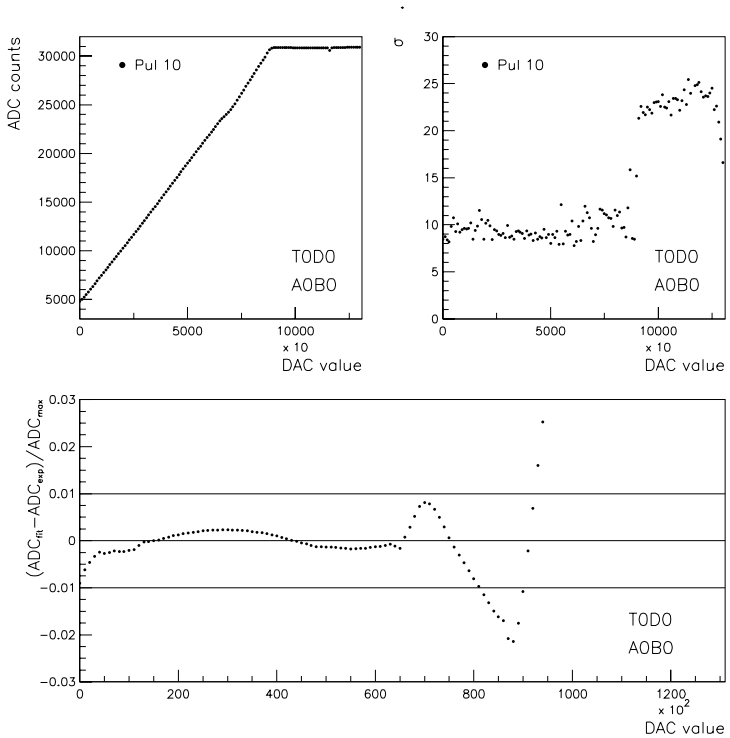

Figure 9: *Linearity of Pulser and Readout Electronics: (a) Mean response of the readout electronics in ADC counts w.r.t. the pulse height in DAC settings (b) σ (c) linearity w.r.t to fit-value.*

due to a 10% variation in the preamplifier input impedance. Relative calibration can be achieved by tuning the calibration pulse timing for the different detector channels.

5.4 Liquid Argon Monitoring

The purity of the liquid argon is critical to the detector performance as electronegative contaminants (e.g. oxygen and nitrogen) can combine with electrons traversing the gap and can severely impact the energy measurement. Radioactive sources are used to monitor these levels. Each of the three calorimeter

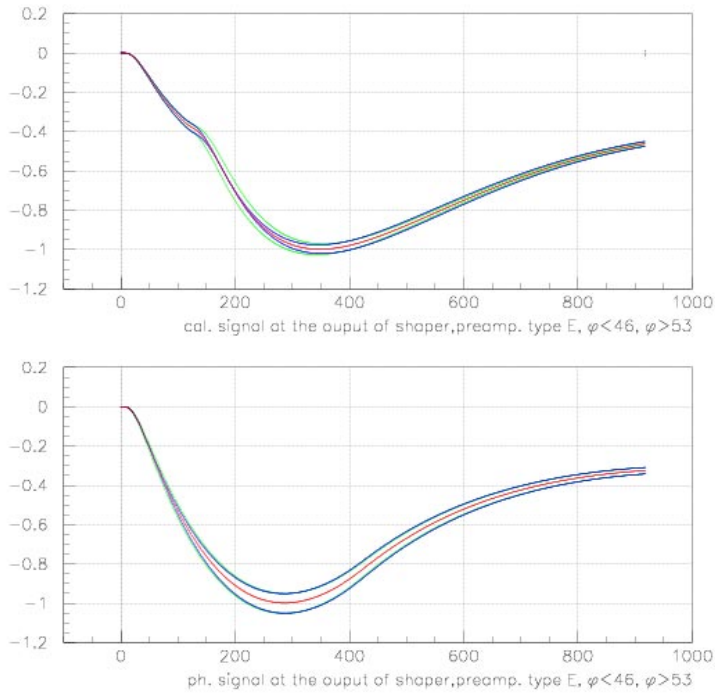

Figure 10: *Comparison of shaper output for calibration signals and physics signals from Spice Simulation. The band shows the variation of the signal due to a* 10% *variation of the preamplifier input impedance.*

cryostats is equipped with four ^{241}Am sources (5 MeV α-particles, 432 yr half-life) with an activity of 0.1 μCi and four ^{106}Ru sources (maximum 3.5 MeV β-particles, ~1 yr half-life). Three of the beta sources in each cryostat now have very low levels of activity ($\leq$ 1 Bq), ten years after the initial detector construction. One slightly stronger source has an activity of about 4 Bq. The charge liberated in the liquid argon gap for the alpha sources is about 4 fC (about 25,000 electrons) and about half this for the beta source. The expected trigger rate is about 500 Hz for the alpha source and 0.3 Hz for the strong beta source.

A new readout board with preamplifier, dual operational-amplifier and

differential driver sends the amplified signals via shielded twisted-pair cable to a differential receiver board to be digitized by a 12-bit ADC using a Xilinx FPGA (Spartan XCS40XL). Histograms can be accumulated very rapidly (few kHz) on the receiver board which are read out via CAN-bus to a PC (running National Instruments LabView). This design is a modification of the liquid argon monitoring system for ATLAS and should be sensitive to less than 1 ppm of oxygen equivalent contamination. This design minimizes the possible introduction of noise into the calorimeter cryostats as no digital electronics is needed on the frontend crates. Ground loops are also prevented using the differential drivers.

The response of the signal is also a function of the liquid argon temperature so this will be monitored as well. The temperatures of the cryostats varied by less than 1% over the course of Run I.

6 Conclusion

The upgraded DØ detector, with new tracking detectors, magnetic field, improved muon coverage and continued excellent performance of the calorimeter, will be able to fully exploit the improved performance of the Tevatron. The new improvements of both detector and machine will allow us to focus on the physics potential at high p_T. Besides the increased discovery potential for the Higgs boson or phenomena beyond the Standard Model, such as supersymmetry or contact interactions, an integrated luminosity of ~ 2 fb^{-1}/year opens the field for extended top quark studies and high precision measurements of electroweak parameters such as the W-mass. With the first 2 fb^{-1}, measurements of the top quark mass and the W-boson mass with uncertainties of 3 GeV and 40 MeV respectively are expected. These precision measurements will narrow the possible parameter space for the Higgs-boson, vital in this post-LEP, pre-LHC era.

Acknowledgments

Many thanks to my DØ colleagues for their great help in getting this manuscript together. Thanks also to the organizers for a very enjoyable conference.

References

1. S. Abachi *et al*, Phys. Rev. Lett. **74**, 2632 (1995).

2. S. Abachi *et al*, Phys. Rev. Lett. **77**, 3309 (1996)
   B. Abbott *et al*, Phys. Rev. Lett. **80**, 3008 (1998), **84**, 222 (2000); Phys. Rev. **D58**, 092003 (1998); **D62**, 092006 (2000).

3. DØ Collaboration, The DØ Upgrade: The Detector and Its Physics, Internal DØ-note (1996),
   http://higgs.physics.lsa.umich.edu/dzero/d0doc96/d0doc.html.

4. M. Adams *et al*, Design Report of the Central Preshower Detector for the DØ Upgrade, Internal DØ-note 3014 (1996).

5. A. Gordeev *et al*, Technical Design Report of the Forward Preshower Detector for the DØ Upgrade, Internal DØ-note (1998).

6. K. Chan *et al*, Electron and Photon Energy Resolution in the Central Calorimeter for Run II, Internal DØ-note 3535 (1998); Electron and Photon Energy Resolution in the End Calorimeters for Run II, Internal DØ-note 3536 (1998).

7. L. Sawyer *et al*, Technical Design Report for the Upgrade of the ICD for DØ Run II, Internal DØ-note 2686 (1997).

8. R. D. Schamberger, The DØ Calorimeter Performance and Calibration, in: Proc. fifth Calorimetry in High Energy Physics (ed. H. Gordon and D. Rueger, Upton, NY, September 1994), 39-50, (World Scientific, 1995).

9. A. Kotwal *et al*, Calorimeter Electronics Upgrade for Run 2. Technical Design Report, Internal DØ-note (1998).